catalysts

MDPI

Article

Dehydrogenative Oxidation of Alcohols Catalyzed by Highly Dispersed Ruthenium Incorporated Titanium Oxide

Youngyong Kim [1], Seokhoon Ahn [2], Jun Yeon Hwang [2], Doo-Hyun Ko [3,*] and Ki-Young Kwon [1,*]

[1] Department of Chemistry, Gyeongsang National University and RINS, Jinju 660-701, Korea; sinionnak@gmail.com

[2] Institute of Advanced Composite Materials, Korea Institute of Science and Technology, Chudong-ro 92, Bongdong-eup, Wanju-gun, Jeonbuk 565-950, Korea; ahn75@kist.re.kr (S.A.); junyeon.hwang@kist.re.kr (J.Y.H.)

[3] Department of Applied Chemistry, Kyung Hee University, 1 Seochun-Dong, Giheung-Gu, Yongin-Si, Gyeonggi-Do 446-701, Korea

* Correspondence: dhko@khu.ac.kr (D.-H.K.); kykwon@gnu.ac.kr (K.-Y.K.); Tel.: +82-31-201-3844 (D.-H.K.); +82-55-772-1493 (K.-Y.K.)

Academic Editors: Albert Demonceau, Ileana Dragutan and Valerian Dragutan
Received: 30 October 2016; Accepted: 21 December 2016; Published: 28 December 2016

Abstract: Ruthenium incorporated titanium oxides (Ru_xTiO_2) were prepared by a one-step hydrothermal method using $Ti(SO_4)_2$ and $RuCl_3$ as the precursor of Ti and Ru, respectively. X-ray diffraction (XRD), X-ray photoelectron spectroscopy (XPS), transmission electron microscope (TEM), Energy-dispersive X-ray spectroscopy (EDS) mapping, and BET were applied for the analyses of catalysts. Ruthenium atoms are well dispersed in the anatase phase of TiO_2 and the crystallite size of Ru_xTiO_2 (≈17 nm) is smaller than that of pure TiO_2 (≈45 nm). In particular, we found that our homemade pure TiO_2 exhibits a strong Lewis acid property. Therefore, the cooperation of ruthenium atoms playing a role in the hydride elimination and the Lewis acid site of TiO_2 can efficiently transfer primary alcohols into corresponding aldehydes in an oxidant-free condition.

Keywords: ruthenium catalyst; titanium oxide; dehydrogenative oxidation

1. Introduction

The oxidation of alcohols into their carbonyl compounds by a cost effective and environmentally benign means is important in synthetic chemistry. Particularly, many researchers have made concentrated efforts on the development of catalytic oxidation reactions using molecular oxygen (O_2) as an oxidant instead of using stoichiometric amounts of expensive and harmful oxidizing reagents [1–3]. Moreover, there have been lots of studies seeking the novel oxidation catalytic systems of alcohols in which alcohol oxidation is accomplished by a dehydrogenation pathway under oxidant-free conditions. In homogeneous catalytic systems, iridium complexes, osmium, or ruthenium pincer-type complexes, and Grubbs' catalyst were commonly applied for the dehydrogenative oxidation [4–7]. Recently, nickel complexes were also reported [8]. In heterogeneous dehydrogenative catalytic systems, mainly noble metals catalysts were reported: alumina-supported silver cluster, hydrotalcite supported silver nanoparticles, ceria supported gold nanoparticles, alumina-supported Pt nanoparticles, alumina-supported Re nanoparticles [9–13]. Particularly, high reactivity was reported for the oxidation of aliphatic alcohols in anaerobic condition [12]. While aerobic oxidation generates water as byproduct, anaerobic conditions produce hydrogen gas. Therefore, the dehydrogenative oxidation prevents the deactivation of catalysts by water and is safely applied to substrates containing water sensitive functional groups.

Nanocrystalline TiO_2 has been intensively investigated in a wide range research fields due to its practical applications, such as photocatalysts, solar cells, materials for water or air purification, and so on [14–17]. It is the chemical, physical, and photo-stability of TiO_2 that all applications mentioned above make possible. Therefore, besides the catalytic properties of TiO_2, it can be a suitable material for supporting catalytic active centers in heterogeneous catalysts. Particularly, TiO_2 supported ruthenium catalysts were utilized for diverse oxidation reactions including aerobic oxidation [18,19], catalytic wet air oxidation of various chemicals [20–22], and electro-oxidation of alcohols [23]. However, to the best of our knowledge, ruthenium incorporated TiO_2 has not been applied to the oxidation of alcohols under oxidant-free conditions. Here we report the dehydrogenative oxidation of benzylic, allylic, and aliphatic alcohols into their corresponding aldehydes using ruthenium incorporated TiO_2 under oxidant-free conditions. We found that benzylic and allylic alcohols exhibited enhanced catalytic activity compared to aliphatic alcohol. Particularly, our homemade pure TiO_2 is a strong Lewis acid catalyst enough to form the Lewis acid-catalyzed Friedel-Craft alkylation products in a benzyl alcohol reaction. Therefore, the dehydrogenative oxidation pathway is accomplished by the synergistic catalysis of the Lewis acidic TiO_2 surface and the highly dispersed ruthenium species acting as the hydride elimination of α-carbon.

2. Results and Discussion

2.1. Catalyst Characterization

Figure 1 shows the crystal phases of ruthenium incorporated titanium oxides (Ru_xTiO_2, x represents the molar ratio of Ru with respect to Ti) obtained by hydrolysis of $Ti(SO_4)_2$ in aqueous solution with the different amount of $RuCl_3$. The pure TiO_2 and Ru_xTiO_2 represent the anatase phase of TiO_2 (JCPDS data file No. 00-21-1272). It was reported that TiO_2 prepared by a hydrothermal method using $Ti(SO_4)_2$ as a precursor exhibited the anatase phase [24]. The reflection peaks originated from RuO_2 are not presented for all the samples obtained from a hydrothermal condition (160 °C). After annealing the $Ru_{0.07}TiO_2$ sample (A-$Ru_{0.07}TiO_2$) at 700 °C for six hours, we find the appearance of Bragg's reflection of RuO_2 (JCPDS file No. 00-040-1290) and phase transformation of TiO_2 from anatase to rutile. This result suggests that ruthenium atoms are randomly incorporated into the crystallite of TiO_2 before annealing. However, the phase segregation of TiO_2 (rutile) and RuO_2 takes place at an elevated temperature. The crystallite sizes of samples in Table 1 was calculated from X-ray line broadening by the Scherrer equation ($D = 0.89\lambda/(\beta\cos\theta)$), where D, λ, β, and θ represent the average crystal size, the Cu Kα wavelength (0.15406 nm), the full-width at half-maximum, and the diffraction angle, respectively. The calculated size of the pure TiO_2 is 26.4 nm which is bigger than that of Ru_xTiO_2 (13–15 nm). The surface area of the pure TiO_2 obtained by the BET method is approximately two-times smaller than that of Ru_xTiO_2 (Table 1).

Table 1. The physical properties of the samples.

Samples	Size (nm)		Surface Area	Ru Content
	XRD	TEM	(m^2/g)	(μmol/g)
Pure TiO_2	26.4	45.7 ± 5.3	48	-
$Ru_{0.01}TiO_2$	13.2	16.7 ± 0.9	104	9
$Ru_{0.03}TiO_2$	13.3	16.9 ± 1.0	111	24
$Ru_{0.05}TiO_2$	13.4	17.0 ± 1.4	125	37
$Ru_{0.07}TiO_2$	14.7	17.3 ± 1.1	126	51

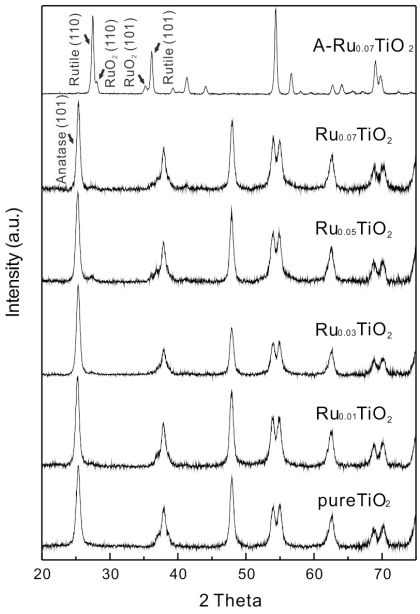

Figure 1. XRD patterns of synthesized Ru_xTiO_2.

The elemental surface analyses of samples were done by X-ray photoelectron spectroscopy (XPS). A survey spectrum verify the presence of titanium, oxygen, ruthenium, and carbon contaminant without other species (Figure S1). The Ru 3d XPS spectra of $Ru_{0.07}TiO_2$ is shown in Figure 2. It is mainly composed of two parts which corresponds to the Ru $3d_{5/2}$ (280.7 eV) and Ru $3d_{3/2}$ (284.6 eV) band originated from spin-orbital coupling. $Ru_{0.07}TiO_2$ was synthesized under highly acidic aqueous conditions because no base was added in the hydrolysis of $Ti(SO_4)_2$. Therefore, we attributed the binding energy of $3d_{5/2}$ (280.7 eV) to the Ru species with +4 oxidation state considering the above mentioned synthetic condition and previous literature data [25–27]. It was known that the Ru $3d_{3/2}$ band overlaps with carbon 1s band and therefore, the Ru $3d_{5/2}$ band is used for quantitative analysis [23,28]. The amount of Ru in $Ru_{0.07}TiO_2$ is 0.58 atomic percent and the ratio of Ru to Ti is 0.026 which is smaller than the added molar ratio (0.07) (In quantitative analysis, the relative sensitivity factor (RSF) of Ti 2p and Ru $3d_{5/2}$ is 2.077 and 2.705, respectively.). The XPS peak intensities of 3d Ru of other Ru_xHAP are too weak to analyze quantitatively.

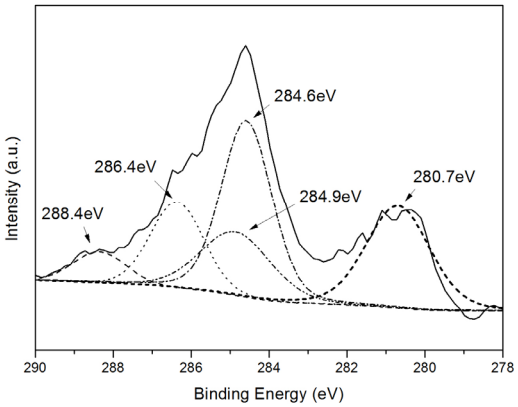

Figure 2. Ru (3d) X-ray photoelectron spectroscopy (XPS) spectrum of the $Ru_{0.07}TiO_2$.

The morphology of samples was characterized by transmission electron microscopy (Figure 3). The pure TiO_2 is similar to corn-shape (Figure 3a). The average size of pure TiO_2 is 45.7 ± 5.3 nm, standard deviation. The shape of Ru_xTiO_2 is similar to pure TiO_2, however, the average size is

smaller, approximately 16–27 nm (Figure 3b,e). This result agrees with the crystallite size calculated by Scherrer's equation based on the full width at half maximum (FWHM) of the (101) facet of anatase. It was reported that the addition of metal ions—such as Na^+, Zn^{2+}, and Fe^{3+}—influence the crystal phase resulting in a decrease of the crystal size of TiO_2 [29–32]. We believe that incorporation of Ru in the TiO_2 lattice causes lattice deformation which might inhibit the crystals growth of TiO_2. After annealing the $Ru_{0.07}TiO_2$ at 700 °C, several crystallites aggregate with each other to be the size of a few hundred nanometers (Figure 3f and Figure S2) with rutile phase. Particularly, dark spots (red circle in Figure 3f) are embedded in the crystallite. These dark spots seem to be RuO_2 crystallites observed in XRD data.

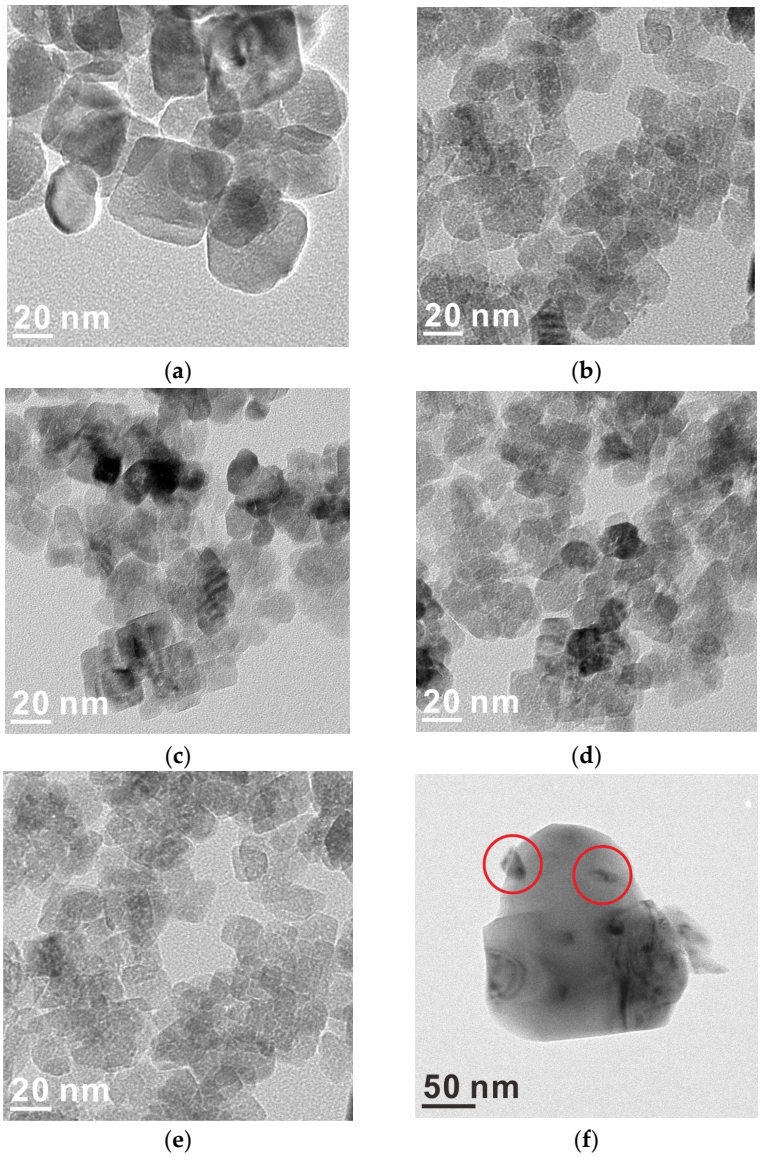

Figure 3. TEM image of Ru_xTiO_2, (**a**) TiO_2; (**b**) $Ru_{0.01}TiO_2$; (**c**) $Ru_{0.03}TiO_2$; (**d**) $Ru_{0.05}TiO_2$; (**e**) $Ru_{0.07}TiO_2$; and (**f**) A-$Ru_{0.07}TiO_2$. Red circles: RuO_2.

The elemental mapping of $Ru_{0.07}TiO_2$ was investigated by energy dispersive X-ray spectroscopy (Figure 4). Individual mapping of Ti, O, and Ru is shown Figure 4b–d, respectively. Figure 4e represents the elemental mapping with Ti, O, and Ru overlaid. We found that Ru is homogeneously dispersed within TiO_2. This result is in good accordance with the previous XRD data of samples in which the reflection peak from RuO_2 does not observed before annealing $Ru_{0.07}TiO_2$. In addition, high resolution

TEM image also showed no aggregation of Ru species (Figure 4f). Therefore, combining XRD and TEM data, we conclude that ruthenium species are highly dispersed in TiO_2 in monomeric form.

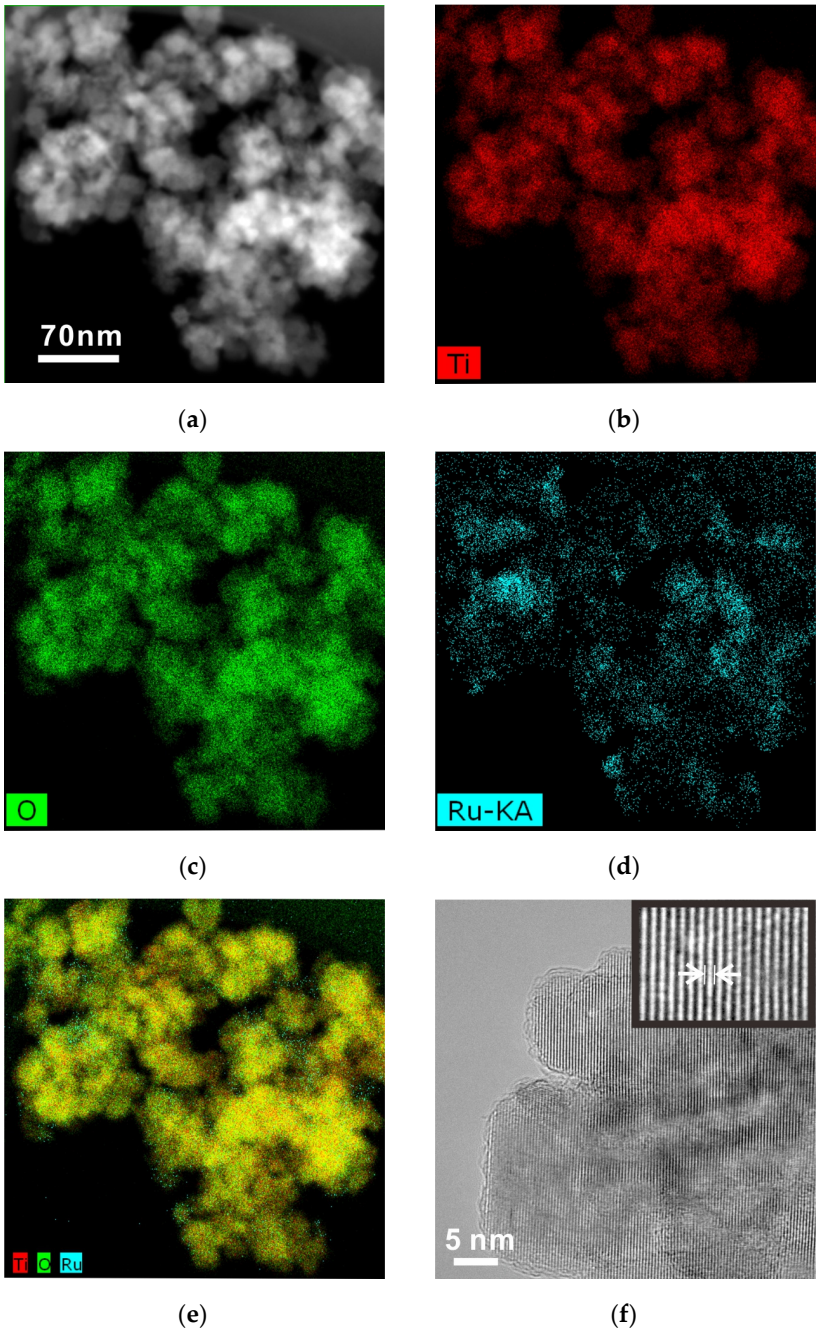

Figure 4. TEM image and Energy-dispersive X-ray spectroscopy (EDS) element mapping of $Ru_{0.07}TiO_2$. (**a**) TEM image of $Ru_{0.07}TiO_2$; (**b**) Ti mapping; (**c**) O mapping; (**d**) Ru mapping; (**e**) overlapping of Ti, O, and Ru; (**f**) high resolution TEM image of $Ru_{0.07}TiO_2$ (insert: interlayer spacing of d(101) = 0.35 nm).

2.2. Catalytic Tests

Catalytic properties were tested by the oxidation reaction of alcohols (benzyl alcohol, cinnamyl alcohol, and 1-octanol) under oxidant-free condition (Table 2). The entries 1–10 showed the oxidative catalytic activities of benzyl alcohol. Compared to the short reaction period (30 min) under O_2 atmosphere (Table 3), reaction time was adjusted to 3 h in N_2 environment. The conversion was less than 2% in the absence of catalyst or in the presence of Degussa, P25 (entries 1 and 2). However,

the conversion of benzyl alcohol with homemade pure TiO_2 (entry 3) was 49% which is high compared to the commercial Degussa P25 (Degussa, Frankfurt, Germany) (entry 2). Importantly, the conversion into benzaldehyde is only 2%. Instead, *o*, *m*, *p*-benzyltoluenes (the molar ratio of ortho/meta/para = 43:6:51) and dibenzyl ether were produced as the major products. These *o*, *m*, *p*-benzyltoluenes were produced by the acid catalyzed Friedel-Crafts alkylation of toluene (solvent) with benzyl alcohol (Figure S3). Dibenzyl ether is produced by the homo-coupling of benzyl alcohol. Both reactions are proceeded by the same intermediate that is benzylic carbocation as indicated in the Scheme 1. Therefore, the surface of homemade pure TiO_2 acts as a Lewis acid catalyst. It was reported that TiO_2 and sulfated TiO_2 are applied to Friedel-Crafts acylation or Beckman rearrangement in which these solid catalysts act as Lewis acid catalysts [33,34]. In the case of Ru_xTiO_2, the major product is benzaldehyde, however, still approximately 7% of benzyl toluene and benzyl ether are remained (entries 4–9). As the Ru content increases, the catalytic activity increases (entries 4–7 in Table 2). For example, $Ru_{0.07}TiO_2$ exhibits 98% conversion with 93% selectivity within 3 h (entry 7). In addition, $Ru_{0.07}TiO_2$ exhibited the catalytic activity to be retained without significant loss for up to three cycles (entries 7–9). However, after annealing $Ru_{0.07}TiO_2$ at 700 °C, the catalytic activity decreased dramatically (entry 10), and the Lewis acid catalyzed products (*o*, *m*, *p*-benzyltoluenes and dibenzyl ether) were not produced by A-$Ru_{0.07}TiO_2$ in the same reaction conditions. Based on the previous mechanistic studies using the single crystal of TiO_2 (typically rutile (110) surface) in vacuum conditions, the reactivity of alcohol on TiO_2 is strongly dependent on the surface defects of TiO_2, such as oxygen vacant sites [35–37]. Besides the reduction of surface area and the aggregation of Ru into RuO_2 during annealing process, the decrease of the surface defects after annealing at 700 °C might result in the low reactivity of A-$Ru_{0.07}TiO_2$.

Table 2. Catalytic properties of alcohol oxidation under oxidant-free conditions [1].

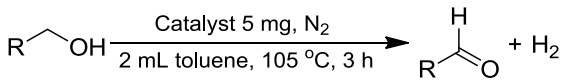

Entry	Catalysts	Substrates	Products	Conversion (%)	Yield to Aldehyde (%)	Selectivity (%)
1	None			0	-	-
2	Degussa, P25			2	1	60
3	pure TiO_2			49	1	2
4	$Ru_{0.01}TiO_2$	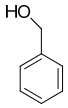	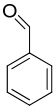	41	34	86
5	$Ru_{0.03}TiO_2$			79	72	93
6	$Ru_{0.05}TiO_2$			88	82	93
7	$Ru_{0.07}TiO_2$			>99	92	93
8	Reuse 7			99	92	93
9	Reuse 8			98	90	92
10	A-$Ru_{0.07}TiO_2$			2	2	99
11	None			0	-	-
12	Degussa, P25	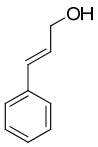	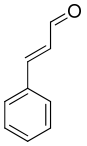	3	3	99
13	pure TiO_2			44	43	98
14	$Ru_{0.01}TiO_2$			78	78	>99
15	$Ru_{0.03}TiO_2$			85	84	>99
16	$Ru_{0.05}TiO_2$			96	94	98
17	$Ru_{0.07}TiO_2$			>99	98	99
18	None			0	-	-
19	Degussa, P25			3	2	93
20	pure TiO_2			4	4	98
21	$Ru_{0.01}TiO_2$			12	12	>99
22	$Ru_{0.03}TiO_2$			23	22	97
23	$Ru_{0.05}TiO_2$			23	22	>99
24	$Ru_{0.07}TiO_2$			24	23	98

[1] Reaction conditions: substrate amount: 0.04 mmol, catalyst amount: 5 mg, reaction time: 3 h, Conversion is calculated by an internal standard method. Yield to aldehyde is calculated by calibration curves (Figure S4). Selectivity is calculated by the peak area of aldehyde divided by the total peak area of product.

Table 3. Catalytic properties of alcohol oxidation using O_2 as an oxidant.

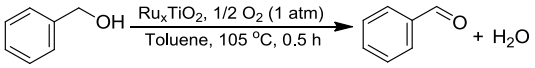

Entry	Catalysts	Substrates	Products	Conversion (%)	Selectivity (%)
1	None			0	-
2	Degussa, P25			3	>99
3	pure TiO_2			3	>99
4	$Ru_{0.01}TiO_2$			38	>99
5	$Ru_{0.03}TiO_2$			77	>99
6	$Ru_{0.05}TiO_2$			94	>99
7	$Ru_{0.07}TiO_2$			>99	>99

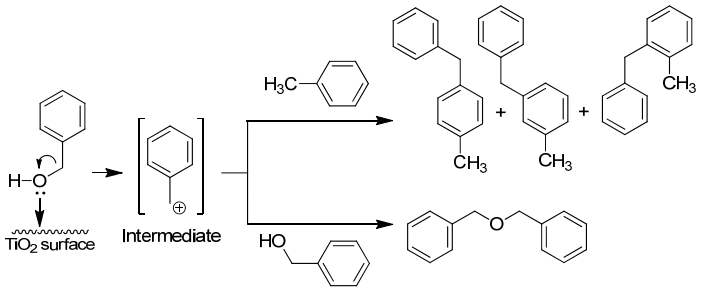

Scheme 1. Lewis acid (TiO_2 surface) catalyzed an electrophilic aromatic substitution and homo-coupling of benzyl alcohol.

Ru_xTiO_2 can be successfully applied oxidation of allylic alcohol (cinnamyl alcohol) into corresponding a α,β-unsaturated carbonyl compound (cinnamaldehyde) with high selectivity (>98%). In the case of cinnamyl alcohol, the by-products from the electrophilic aromatic substitution or acid catalyzed homo-coupling were not produced (entries 14–17 in Table 2). Similar to benzyl alcohol oxidation, homemade pure TiO_2 showed the high conversion compared to Degussa, P25 (entries 12 and 13 in Table 2). In addition, pure TiO_2 exhibits high selectivity in transformation into the cinnamaldehyde (entry 13 in Table 2). We want to point out that the conversion of alcohol into aldehyde in our catalytic system is not a common phenomenon because the dehydration of various alcohols into alkenes is a more general reaction on TiO_2 surface instead of dehydrogenation reaction [35,38]. Unfortunately, the kinetics of primary aliphatic alcohol (1-octanol) were not as efficient as that of benzyl alcohol and cinnamyl alcohol in the given conditions (entries 19–24 in Table 2). In the case of the oxidation of secondary alcohol (1-phenyl ethanol), the major product is styrene instead of acetophenone, which indicates that secondary benzylic alcohols are prone to elimination under the same experimental conditions (Table S1).

In our initial experiment set-up, the role of TiO_2 is catalytic supports to incorporate ruthenium atoms that are catalytic active centers. However, our homemade TiO_2 itself significantly involves in the reaction (entries 3 and 13 in Table 2). For the conversion of alcohol into aldehyde, two hydrogen atoms (one is attached to oxygen, the other is attached to α-carbon) are detached. A previous high resolution STM study verified that adsorption process of alcohol on TiO_2 surface induces the detachment of the hydroxyl hydrogen in which the regular surface Ti sites of TiO_2 enable alcohols to be adsorbed molecularly and dissociatively (deprotonated alkoxide) at room temperature [37]. Particularly, our homemade highly acidic surface of pure TiO_2 facilitates alcohol adsorption on the surface to form deprotonated alkoxide species. The hydrogen elimination of the α-carbon seems to take place on exclusively ruthenium species (Figure 5). This interpretation is supported by a dramatic change of major products from *o*, *m*, *p*-benzyltoluenes to benzaldehyde when pure TiO_2 is replaced $Ru_{0.01}TiO_2$ (entries 3 and 4 in Table 2). Similarly, Yamaguchi et al. proposed that in an alcohol oxidation reaction on Ru_xTiO_2 using molecular oxygen as oxidant, the reaction was accomplished by

the ruthenium alcoholate formation followed by hydride elimination and the rate determining step is the hydride abstraction step [18].

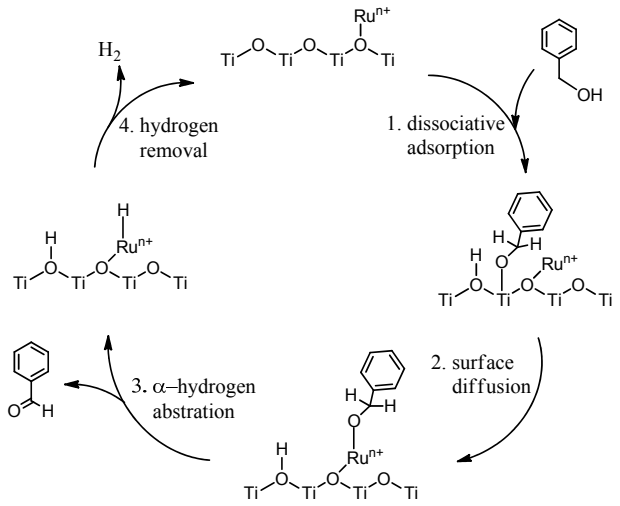

Figure 5. The proposed mechanism for the dehydration of benzyl alcohol by Ru_xTiO_2.

The turnover frequency (*TOF*) based on Ru for benzyl alcohol oxidation using $Ru_{0.01}TiO_2$ amounts to 130 h^{-1} where the total amount of ruthenium obtained from Inductively coupled plasma mass spectrometry (ICP) data are used for *TOF* calculation. In comparison with other heterogeneous catalytic systems in oxidant-free conditions (Au/CeO_2, (*TOF* = 125 h^{-1}) [7], Ag/Al_2O_3 (>2 h^{-1}) [9], Ru/AlO(OH) (7 h^{-1}) [39], Cu/hydrotalcite (1.5 h^{-1}) [40], Cu/Al_2O_3 (8.3 h^{-1}) [41]), our value is higher except for the silver nanoparticles on the hydrotalcite system (590 h^{-1}) [11].

3. Materials and Methods

3.1. Synthesis of TiO_2 and Ruthenium-Incorporated TiO_2 (Ru_xTiO_2)

$Ti(SO_4)_2$ and $RuCl_3$ nH_2O were purchased from Kanto and Sigma-Aldrich, respectively. TiO_2 and Ru_xTiO_2 were synthesized by a hydrothermal method using $Ti(SO_4)_2$ and $RuCl_3$ nH_2O as the precursor of Ti and Ru, respectively. 15 mL of 24% $Ti(SO_4)_2$ (Ti: 20 mmol) was added dropwise into the 60 mL of aqueous solution containing the different amount of $RuCl_3$ (Ru: 0, 0.2, 0.6, 1, 1.4 mmol) under vigorous stirring. The samples are labeled Ru_xTiO_2, in which *x* represents the mole ratio of ruthenium with respect to titanium. The solution was transferred to a Teflon-lined autoclave reactor and treated at 160 °C for 6 h. After the reaction vessel was cooled down to room temperature, the samples were separated by centrifugation and purified by washing with distilled water three times. Finally, the precipitates were obtained by drying under vacuum at room temperature. A-$Ru_{0.07}TiO_2$ was prepared by annealing the $Ru_{0.07}TiO_2$ at 700 °C for 6 h.

3.2. Characterization of Catalysts

X-ray diffraction (XRD) patterns were obtained using a Bruker D8 Advance X-ray diffractometer with Cu Kα radiation (Bruker, Karlsruhe, Germany). Diffraction patterns were taken over the 2θ range 20°–75°. The XPS results were obtained on a PHI 5000 Versaprobe instrument (ULVAC-PHI Inc., Chigasaki, Japan) in which monochromated Al Kα radiation (hν = 1486.6 eV) is illuminated as the light source. The X-ray anode was run at 25 W and the voltage was maintained at 15 kV. The pass energy was fixed at 23.5 eV to ensure sufficient resolution to determine peak positions accurately. The binding energies were calibrated by using the Au $4f_{7/2}$ signal at 84.0 eV. The prepared sample morphology was characterized by a TITAN G2 60-300 (FEI, Hillsboro, OR, USA) transmission electron microscopy (TEM) equipped with CETCOR corrector and 4-silicon drift detector system energy dispersive X-ray

spectroscopy (Super-X EDS, Bruker) operating at an accelerating voltage of 80 kV. The quantitative EDS area mapping was carried out using a scanning electron probe (Bruker) with a size of 1 nm over the sample. The surface area of samples was measured by Brunauer-Emmett-Teller (BET) method. N_2 adsorption-desorption isotherms of samples at liquid nitrogen temperature (77 K) were obtained using Belsorp Mini II (BEL Japan, Osaka, Japan).

3.3. Catalytic Tests

2 mL of alcohols (benzyl alcohol, 1-octanol, cynnamyl alcohol, 20 mM) dissolved in toluene was added to 16 mL test tubes containing 5 mg of catalysts. To ensure oxygen-free conditions, nitrogen gas was flowed for 20 min in the reaction mixture for degassing, followed by connection of an N_2 balloon that was connected to a syringe needle, which was inserted into the septum covering the test tube. The reaction mixture was heated 105 °C for 3 h. After cooling the reaction mixture to room temperature, the solid catalysts were separated from solution phase by centrifugation. The solution phase was analyzed by gas chromatography (GC, aglient 7890A, Agilent Technologies, Santa Clara, CA, USA) with a flame ionization detector (FID). Dodecane was used as an internal standard for the calculation of conversion. The catalytic property of the commercial Degussa P25 was also tested for comparison.

4. Conclusions

In summary, we prepared the highly dispersed ruthenium incorporated TiO_2 by a one-pot hydrothermal method. Ru_xTiO_2 can transfer the benzylic, allylic, and alkyl alcohols into corresponding carbonyl compounds in oxidant-free conditions. In our catalytic system, particularly, TiO_2 acts as not only the catalytic support but also a Lewis acid catalytic site which improves reactivity by facilitating the deprotonated adsorption of alcohols on the catalysts. Therefore, the synergistic effect of hydride elimination by ruthenium and the Lewis acid site on TiO_2 can efficiently transfer primary alcohols into corresponding aldehydes in oxidant-free conditions.

Supplementary Materials: The following are available online at http://www.mdpi.com/2073-4344/7/1/7/s1, Figure S1: The survey XPS spectrum of $Ru_{0.07}TiO_2$, Figure S2: TEM image of A-$Ru_{0.07}/TiO_2$. After annealing, crystallites aggregate each other to form large crystallites without particular shape. (**a**) TEM image; (**b**) aggregation of crystallites, Figure S3: (**Top**) Conversion data from analysis of gas chromatography (GC, Agilent 7890A, Agilent Technologies, Santa Clara, CA, USA). Dodecane was used as internal standard for the calculation of conversion (**middle**); the main products by pure TiO_2 were *o*, *m*, *p*-benzyltoluenes which are produced by Friedel-Crafts alkylation of toluene (solvent) with benzyl alcohol. In addition dibenzyl ether is also produced by the acid catalyzed homo-coupling of benzyl alcohol (**bottom**), Figure S4: The calibration curves of alcohols and aldehydes. The flame ionization detector was used. (**a**) Benzyl alcohol and benzaldehyde; (**b**) 1-octanol and 1-octanal; (**c**) cinnamyl alcohol and cinnamaldehyde, Table S1: Catalytic properties of 1-phenyl ethanol oxidation under oxidant-free condition.

Acknowledgments: Ki-Young Kwon acknowledges that this research was supported by the Creative Human Resource Training Project for Regional Innovation through the National Research Foundation of Korea (NRF) funded by the Ministry of Education (NRF-2015H1C1A1035812).

Author Contributions: Ki-Young Kwon and Doo-Hyun Ko conceived and designed the experiments; Youngyong Kim performed syntheses of catalysts and the evaluation of catalytic properties; Seokhoon Ahn and Jun Yeon Hwang contributed TEM experiments; Ki-Young Kwon and Youngyong Kim wrote the paper.

Conflicts of Interest: The authors declare no conflict of interest.

References

1. Dijksman, A.; Marino-González, A.; Payeras, A.M.; Arends, I.W.C.E.; Sheldon, R.A. Efficient and selective aerobic oxidation of alcohols into aldehydes and ketones using ruthenium/TEMPO as the catalytic system. *J. Am. Chem. Soc.* **2001**, *123*, 6826–6833. [CrossRef] [PubMed]
2. Yamaguchi, K.; Mizuno, N. Efficient heterogeneous aerobic oxidation of amines by a supported ruthenium catalyst. *Angew. Chem. Int. Ed.* **2003**, *42*, 1480–1483. [CrossRef] [PubMed]

3. Mori, K.; Hara, T.; Mizugaki, T.; Ebitani, K.; Kaneda, K. Hydroxyapatite-supported palladium nanoclusters: A highly active heterogeneous catalyst for selective oxidation of alcohols by use of molecular oxygen. *J. Am. Chem. Soc.* **2004**, *126*, 10657–10666. [CrossRef] [PubMed]
4. Fujita, K.I.; Tanino, N.; Yamaguchi, R. Ligand-promoted dehydrogenation of alcohols catalyzed by Cp*Ir complexes. A new catalytic system for oxidant-free oxidation of alcohols. *Org. Lett.* **2007**, *9*, 109–111. [CrossRef] [PubMed]
5. Bertoli, M.; Choualeb, A.; Lough, A.J.; Moore, B.; Spasyuk, D.; Gusev, D.G. Osmium and ruthenium catalysts for dehydrogenation of alcohols. *Organometallics* **2011**, *30*, 3479–3482. [CrossRef]
6. Adair, G.R.A.; Williams, J.M.J. Oxidant-free oxidation: Ruthenium catalysed dehydrogenation of alcohols. *Tetrahedron Lett.* **2005**, *46*, 8233–8235. [CrossRef]
7. Baratta, W.; Bossi, G.; Putignano, E.; Rigo, P. Pincer and diamine Ru and Os diphosphane complexes as efficient catalysts for the dehydrogenation of alcohols to ketones. *Chem. Eur. J.* **2011**, *17*, 3474–3481. [CrossRef] [PubMed]
8. Chakraborty, S.; Piszel, P.E.; Brennessel, W.W.; Jones, W.D. A single nickel catalyst for the acceptorless dehydrogenation of alcohols and hydrogenation of carbonyl compounds. *Organometallics* **2015**, *34*, 5203–5206. [CrossRef]
9. Shimizu, K.I.; Sugino, K.; Sawabe, K.; Satsuma, A. Oxidant-free dehydrogenation of alcohols heterogeneously catalyzed by cooperation of silver clusters and acid-base sites on alumina. *Chem. Eur. J.* **2009**, *15*, 2341–2351. [CrossRef] [PubMed]
10. Wang, M.; Wang, F.; Ma, J.; Li, M.; Zhang, Z.; Wang, Y.; Zhang, X.; Xu, J. Investigations on the crystal plane effect of ceria on gold catalysis in the oxidative dehydrogenation of alcohols and amines in the liquid phase. *Chem. Commun.* **2014**, *50*, 292–294. [CrossRef] [PubMed]
11. Mitsudome, T.; Mikami, Y.; Funai, H.; Mizugaki, T.; Jitsukawa, K.; Kaneda, K. Oxidant-free alcohol dehydrogenation using a reusable hydrotalcite-supported silver nanoparticle catalyst. *Angew. Chem. Int. Ed.* **2008**, *47*, 138–141. [CrossRef] [PubMed]
12. Kon, K.; Hakim Siddiki, S.M.A.; Shimizu, K.I. Size- and support-dependent Pt nanocluster catalysis for oxidant-free dehydrogenation of alcohols. *J. Catal.* **2013**, *304*, 63–71. [CrossRef]
13. Kon, K.; Onodera, W.; Toyao, T.; Shimizu, K.I. Supported rhenium nanoparticle catalysts for acceptorless dehydrogenation of alcohols: structure-activity relationship and mechanistic studies. *Catal. Sci. Technol.* **2016**, *6*, 5864–5870. [CrossRef]
14. Konstantinou, I.K.; Albanis, T.A. TiO_2-assisted photocatalytic degradation of azo dyes in aqueous solution: Kinetic and mechanistic investigations: A review. *Appl. Catal. B* **2004**, *49*, 1–14. [CrossRef]
15. Al-Ekabi, H.; Serpone, N. Kinetic studies in heterogeneous photocatalysis. 1. Photocatalytic degradation of chlorinated phenols in aerated aqueous solutions over TiO_2 supported on a glass matrix. *J. Phys. Chem.* **1988**, *92*, 5726–5731. [CrossRef]
16. O'Regan, B.; Grätzel, M. A low-cost, high-efficiency solar cell based on dye-sensitized colloidal TiO_2 films. *Nature* **1991**, *353*, 737–740. [CrossRef]
17. Tang, J.; Durrant, J.R.; Klug, D.R. Mechanism of photocatalytic water splitting in TiO_2. Reaction of water with photoholes, importance of charge carrier dynamics, and evidence for four-hole chemistry. *J. Am. Chem. Soc.* **2008**, *130*, 13885–13891. [CrossRef] [PubMed]
18. Yamaguchi, K.; Kim, J.W.; He, J.; Mizuno, N. Aerobic alcohol oxidation catalyzed by supported ruthenium hydroxides. *J. Catal.* **2009**, *268*, 343–349. [CrossRef]
19. Köckritz, A.; Sebek, M.; Dittmar, A.; Radnik, J.; Brückner, A.; Bentrup, U.; Pohl, M.M.; Hugl, H.; Mägerlein, W. Ru-catalyzed oxidation of primary alcohols. *J. Mol. Catal. A* **2006**, *246*, 85–99. [CrossRef]
20. Grosjean, N.; Descorme, C.; Besson, M. Catalytic wet air oxidation of N,N-dimethylformamide aqueous solutions: Deactivation of TiO_2 and ZrO_2-supported noble metal catalysts. *Appl. Catal. B* **2010**, *97*, 276–283. [CrossRef]
21. Besson, M.; Descorme, C.; Bernardi, M.; Gallezot, P.; Di Gregorio, F.; Grosjean, N.; Pham Minh, D.; Pintar, A. Supported noble metal catalysts in the catalytic wet air oxidation of industrial wastewaters and sewage sludges. *Environ. Technol.* **2010**, *31*, 1441–1447. [CrossRef] [PubMed]
22. Pintar, A.; Batista, J.; Tišler, T. Catalytic wet-air oxidation of aqueous solutions of formic acid, acetic acid and phenol in a continuous-flow trickle-bed reactor over Ru/TiO_2 catalysts. *Appl. Catal. B* **2008**, *84*, 30–41. [CrossRef]

23. Buonaiuto, M.; De Crisci, A.G.; Jaramillo, T.F.; Waymouth, R.M. Electrooxidation of alcohols with electrode-supported transfer hydrogenation catalysts. *ACS Catal.* **2015**, *5*, 7343–7349. [CrossRef]
24. Park, H.K.; Moon, Y.T.; Kim, D.K.; Kim, C.H. Formation of monodisperse spherical TiO_2 powders by thermal hydrolysis of $Ti(SO_4)_2$. *J. Am. Ceram. Soc.* **1996**, *79*, 2727–2732. [CrossRef]
25. Paunović, P.; Gogovska, D.S.; Popovski, O.; Stoyanova, A.; Slavcheva, E.; Lefterova, E.; Iliev, P.; Dimitrov, A.T.; Jordanov, S.H. Preparation and characterization of Co-Ru/TiO_2/MWCNTs electrocatalysts in PEM hydrogen electrolyzer. *Int. J. Hydrogen Energy* **2011**, *36*, 9405–9414. [CrossRef]
26. Lin, X.; Yang, K.; Si, R.; Chen, X.; Dai, W.; Fu, X. Photo-assisted catalytic methanation of CO in H_2-rich stream over Ru/TiO_2. *Appl. Catal. B* **2014**, *147*, 585–591. [CrossRef]
27. Rizzi, G.A.; Magrin, A.; Granozzi, G. Substitutional $Ti_{(1-x)}Ru_xO_2$ surface alloys obtained from the decomposition of $Ru_3(CO)_{12}$ on TiO_2(110). *Phys. Chem. Chem. Phys.* **1999**, *1*, 709–711. [CrossRef]
28. Di, L.; Wu, G.; Dai, W.; Guan, N.; Li, L. Ru/TiO_2 for the preferential oxidation of CO in H_2-rich stream: Effects of catalyst pre-treatments and reconstruction of Ru sites. *Fuel* **2015**, *143*, 318–326. [CrossRef]
29. Luo, J.; Yang, X.; Li, D. Preparation of TiO_2 nanoparticles doped with Cs^+ and Sr^{2+} and their photocatalytic activity under solar light. *Adv. Mat. Res.* **2010**, *113*, 1945–1950. [CrossRef]
30. Nam, H.J.; Amemiya, T.; Murabayashi, M.; Itoh, K. The influence of Na^+ on the crystallite size of TiO_2 and the photocatalytic activity. *Res. Chem. Intermed.* **2005**, *31*, 365–370. [CrossRef]
31. Devi, L.G.; Murthy, B.N.; Kumar, S.G. Photocatalytic activity of TiO_2 doped with Zn^{2+} and V^{5+} transition metal ions: Influence of crystallite size and dopant electronic configuration on photocatalytic activity. *Mater. Sci. Eng. B* **2009**, *166*, 1–6. [CrossRef]
32. Safari, M.; Talebi, R.; Rostami, M.H.; Nikazar, M.; Dadvar, M. Synthesis of iron-doped TiO_2 for degradation of reactive Orange16. *J. Environ. Sci. Eng.* **2014**, *12*. [CrossRef] [PubMed]
33. Su, K.; Li, Z.; Cheng, B.; Zhang, L.; Zhang, M.; Ming, J. The studies on the Friedel-Crafts acylation of toluene with acetic anhydride over HPW/TiO_2. *Fuel Process. Technol.* **2011**, *92*, 2011–2015. [CrossRef]
34. Hosseini-Sarvari, M.; Safary, E. Nano-sulfated titania (TiO_2/SO_{2-4}) as a new solid acid catalyst for Friedel-Crafts acylation and Beckman rearrangement in solvent-free conditions. *J. Sulfur Chem.* **2011**, *32*, 463–473. [CrossRef]
35. Farfan-Arribas, E.; Madix, R.J. Role of defects in the adsorption of aliphatic alcohols on the TiO_2(110) surface. *J. Phys. Chem. B* **2002**, *106*, 10680–10692. [CrossRef]
36. Chen, L.; Li, Z.; Smith, R.S.; Kay, B.D.; Dohnálek, Z. Conversion of 1,2-propylene glycol on rutile TiO_2(110). *J. Phys. Chem. C* **2014**, *118*, 15339–15347. [CrossRef]
37. Hansen, J.Ø.; Huo, P.; Martinez, U.; Lira, E.; Wei, Y.Y.; Streber, R.; Lægsgaard, E.; Hammer, B.; Wendt, S.; Besenbacher, F. Direct evidence for ethanol dissociation on rutile TiO_2(110). *Phys. Rev. Lett.* **2011**, *107*, 136102. [CrossRef] [PubMed]
38. Kim, Y.K.; Kay, B.D.; White, J.M.; Dohnálek, Z. Alcohol chemistry on rutile TiO_2(110): The influence of alkyl substituents on reactivity and selectivity. *J. Phys. Chem. C* **2007**, *111*, 18236–18242. [CrossRef]
39. Kim, W.H.; Park, I.S.; Park, J. Acceptor-free alcohol dehydrogenation by recyclable ruthenium catalyst. *Org. Lett.* **2006**, *8*, 2543–2545. [CrossRef] [PubMed]
40. Mitsudome, T.; Mikami, Y.; Ebata, K.; Mizugaki, T.; Jitsukawa, K.; Kaneda, K. Copper nanoparticles on hydrotalcite as a heterogeneous catalyst for oxidant-free dehydrogenation of alcohols. *Chem. Commun.* **2008**, *39*, 4804–4806. [CrossRef] [PubMed]
41. Damodara, D.; Arundhathi, R.; Likhar, P.R. Copper nanoparticles from copper aluminum hydrotalcite: An efficient catalyst for acceptor- and oxidant-free dehydrogenation of amines and alcohols. *Adv. Synth. Catal.* **2014**, *356*, 189–198. [CrossRef]